

Experimental Study and Artificial Neural Networks Prediction of Effective Parameters in Continuous Dieless Wire Drawing Process

Rafid Jabbar Mohammed
Mech. Engineering Dept.
University of Basrah
Basrah
rafidalsukaini@gmail.com

Jaafar Khalaf Ali
Mech. Engineering Dept.
University of Basrah
Basrah
jaafarkhalaf@gmail.com

Ameen Ahmed Nassar
Mech. Engineering Dept.
University of Basrah
Basrah
aaledani@gmail.com

Abstract- The dieless drawing process is an innovative method emanated and appeared in coincidence with development of the concept of metal superplasticity. It is utilized from the local heating of a wire or tube to a specified temperature and followed by a local cooling, so an additional deformation is inhibited. In this study, a special dieless drawing machine was designed to carry out an experimental program on SUS304-stainless steel wire having diameter of (1.6-2) mm to investigate the main process parameters such as speeds, heat quantity, heating coil width and heating-cooling separation distance. Also, a numerical model based on thermo-mechanical analysis was developed and validated with experimental program. Furthermore, an artificial neural network ANN model based on current experimental data was prepared to predict the dieless drawing behavior. A maximum area reduction of 40.7% was obtained in single pass. A 3.12mm/s feeding velocity and 4.97mm/s drawing velocity were realized through the experimental tests. The results showed that both drawing force and wire profile were effected by increasing of feeding speed, heating coil width and separation distance. Also, it is confirmed that strain rate was reduced by increasing the heating coil width and the reduction ratio was promoted. A maximum error of 21% was recorded between ANN model and experimental results. The results showed a good agreement among experimental, numerical and ANN models.

Keywords: Dieless wire drawing, experimental tests, artificial neural network prediction.

Nomenclature:

T_m : material melting temperature ($^{\circ}\text{K}$).

HFIH: high frequency induction heating.

DLD: dieless drawing.

V_o : feeding velocity (mms^{-1}) or heating-cooling units speed.

V_1 : drawing velocity (mms^{-1}), k , and C_p

ρ : material density (kg/m^3).

k : thermal conductivity (W/m.K).

C_p : specific heat (J/kg.K).

T : temperature ($^{\circ}\text{K}$).

T_{\max} : maximum temperature ($^{\circ}\text{K}$).

T_{sp} : setpoint temperature ($^{\circ}\text{K}$).

T_o : ambient temperature ($^{\circ}\text{K}$).

λ : Thermal diffusivity (m^2/s).

d_o : initial wire diameter (mm).

d_1 : final wire diameter (mm).

A_o : initial wire cross-section area (m^2).

A_1 : final wire cross-section area (m^2).

A : instantaneous wire cross-section area (m^2).

R_o : initial wire radius (m).

R : instantaneous radius (m).

R_1 : final wire radius (m).

P : heat quantity (W/m^2).

h : heat transfer coefficient ($\text{W/m}^2.\text{K}$).

h_a : heat transfer coefficient outside cooling unit ($\text{W/m}^2.\text{K}$).

h_c : heat transfer coefficient inside cooling unit ($\text{W/m}^2.\text{K}$).

z : axial (longitudinal) coordinate (m).

r : radial coordinate (m).

F_d : drawing force (N).

L_D : deformation length (m).

L : total length (m).

H-C: distance between heating and cooling units (m).

h_z : location of heating coil (m).

h_w : heating coil width (m).

c_w : width of cooling unit (m).

c_z : location of cooling unit (m).

c_e : distance which is affected by cooling air (m).

q : heat flux supplied by induction coil (W/m^2).

q_{meas} : heat flux measured on the sleeve (W/m^2).

N : number of elements in finite difference approximation.

Δz : element increment.

K : strength coefficient (N/m^2).

n : strain hardening exponent.

m : strain rate sensitivity index.

σ : instantaneous plastic flow stress (N/m^2).

σ_o : elastic flow stress at start of deformation.

σ_1 : elastic flow stress at end of deformation.

ϵ : plastic strain.

ϵ_o : initial strain.

$\dot{\epsilon}$: strain rate (1/s).

ϵ_o : scaling factor (1/s).

RA: area reduction ratio.

HP: horse power.

TH: thermocouple.

1. INTRODUCTION

There is an innovative technique has been emerged and developed through the last four decades for drawing the wires and tubes in the absence of traditional dies, namely, (DLD) dieless drawing process. This process depends on local heating of a specified length of the wire/tube followed by a local cooling and coincidence with apply a suitable

feeding and drawing speeds to create proper drawing force. Fig.1 shows types of dieless drawing process. The main issue in this process is instability (unevenness of the final product) and low productivity. This is emanated from the complicated interdependent among the process parameters as pointed out by the authors whose worked on this process [10]. Many workers have investigated extensively dieless drawing parameters theoretically and experimentally and reported that control of deformation temperature (heating stage) within the range of $(0.4-0.5)T_m$ along with appropriate applied velocities can lead to more stability of dieless drawing [18].

Earliest, Alexander and Turner [1], conducted an extensive experiments on mild steel rod having 50mm and 76mm in diameters, Niobium mild steel having 25mm in diameter, stainless steel 8/17 Ni-Cr having 50mm and 38mm in diameters, chrome steel having 38mm, 50mm and 57mm in diameters and Titanium alloy having 25mm in diameters. They used high frequency induction heating (HFIH) with non-continuous dieless machine at 1.3 mm/s drawing speed. The workability of stainless steel 304, pure titanium and carbon steel all have an outer diameter of 8mm at drawing velocity of 0.833mm/s heated by HFIH with non-continuous dieless machine were investigated by Sekiguchi et al. [2]. Hashmi et al. [3], utilized the molten polymer to dielessly draw the copper wire of diameter 1.625mm and achieved up to 21% area reduction. Weidig et al. [4] performed an experimental tests on non-continuous dieless machine with induction heating and specific cooling method to study the microstructure of low carbon steel C15 rod which has diameter of 16mm. Pawelski et al [5] carried out an experimental program on non-continuous dieless machine with induction heating and control system to examine the process variables – feeding velocity and drawing force – for C45 and 115-Cr-V3 steels. Fann et al. [6] developed a numerical model to predict the evolution of temperature profile and drawing force for SUS304-stainless steel-wire having 5 mm in diameter. Hwang and Kuo [7] implemented an experimental tests on non-continuous DLD machine as well as finite element procedure to investigate the main parameters like deforming velocity and temperature and its effects on workability limit of SUS304 tube which has outside diameter/thickness of 6.35 mm and 1mm respectively at heating width of 5mm. They accomplished up to 40% area reduction at 0.8mm/s drawing speed. Hwang et al. [8] used the same procedures and the same material as in [7] but at heating width of 10mm and they accomplished up to 50% area reduction at 0.4mm/s drawing speed. Wang et al.[9] studied experimentally the wall thickness variation of the stainless steel tubes have different sizes. They concluded that variation of wall thickness is increased with increasing of reduction ratio and is decreased with increasing the distance between heating and cooling units. Tiernan and Hillery [10] developed a continuous dieless drawing machine utilized induction heating alongside mathematical model and finite element simulation to study DLD parameters process for low carbon steel wire which has diameter of 2.65mm. They observed that variation of wire diameter is affected by reduction ratio and there is intricate inter-dependency among the process variables. Huh et al. [11] designed a continuous DLD machine utilized microwaves as heating source to investigate the relationship between diameter variation and drawing ratio of SUS304 wire having diameter of

0.975mm. Naughton and Tiernan [12, 13] conducted an experimental tests with mathematical modelling on titanium wire alloy which has diameter of 2.36mm to study process parameters like reduction ratio, separation length between heating and cooling devices and their effects on variation of final diameter. They achieved up to 40% and 36% reduction ratio respectively. Furushima et al. [14] studied experimentally the influence of feeding velocity and heating conditions on temperature radius profiles under control of drawing velocity.

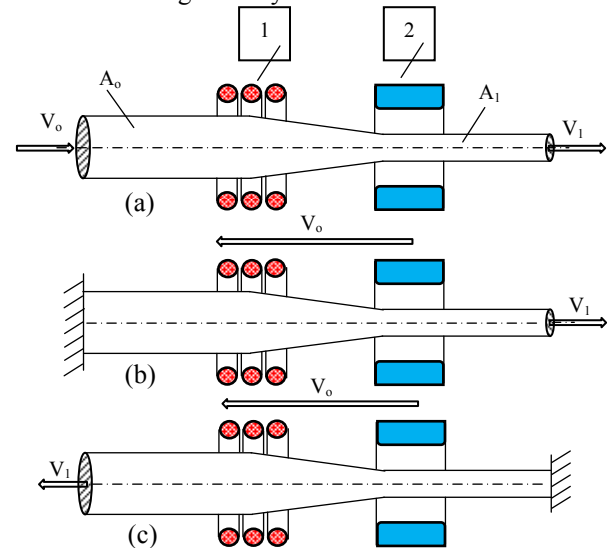


Fig. 1: The Variant Types of DLD Process, (a) Continuous, (b) and (c) Non Continuous. 1-Heating Unit; 2- Cooling Unit.

They used SUS304 tube having 1.5mm diameter and 0.3mm thickness with a continuous DLD machine. T. Furushima et al [15] accomplished of 40% area reduction by means of the laser technique for microtube SUS304 which has 0.5mm outer diameter and 0.13mm thickness at drawing velocity of 1.67mm/s. Effect of DLD variables such as forming speeds, temperature status, material thermal properties and geometrical variables on final area and temperature profiles were studied analytically by Hongyu et al. [16]. Furushima and Manabe [17] utilized a mandrel-DLD continuous process with HFIH and water cooling to manufacture a magnesium alloy tubes from the original dimensions (5mm outer diameter and 1.5mm thickness) to the final size (3.35mm diameter and 0.69mm thickness) over multi-pass drawing. They achieved up to 58.1% reduction ratio at feeding and drawing speeds of 0.5mm/s and 1.2mm/s respectively.

In this study, a numerical model consists of two parts: heat transfer and deformation analysis was setup to predict the temperature and diameter profiles for SUS304 wire having original diameter of (1.6-2) mm through dieless drawing process. To validate the numerical results, a continuous DLD machine was designed, constructed and commissioned in the mechanical engineering department at University of Basrah, to study the effective parameters of DLD process. Also, an artificial neural network ANN model was developed based on obtained experimental data to predict the behavior of DLD process.

2. NUMERICAL MODEL

During the plastic deformation at elevated temperatures as in dieless drawing process, the thermo-mechanical analysis is indispensable so as temperature effects are implied in the deformation process [18, 19]. So, this model is composed of two models, namely, heat model to calculate temperature distribution along the wire and determine the heat flux corresponding to maximum temperature reached. Then, the temperatures distribution is used as input to the second model, namely, deformation to predict the final diameter profile and determine the drawing force required.

2.1 HEAT TRANSFER MODEL

The one dimensional, steady state, heat conduction equation including convection term equation (1) is formulated by means of finite difference-central approximation and solved by MatLab. The postulates for this model are follows:

1. Temperature is function of the wire axial coordinate only.
2. The process is steady and axisymmetric [19].
3. Electromagnetic effects are not considered here.
4. The thermal properties ρ , k , and C_p are temperature independent, i.e., isotropic material.
5. Effect of reduction of the cross-section area on temperature profile is disregarded [20].

By ignoring the heat generated by the plastic deformation, the heat balance during dieless drawing process is governed by the following equation [20, 21]: where: $\lambda=k/C_p\rho$

$$\frac{d^2T}{dz^2} - \frac{V_o}{\lambda} \frac{dT}{dz} + \frac{2\pi R_o}{A_o k} P - \frac{2\pi R_o h}{A_o k} (T - T_o) = 0 \tag{1}$$

The heat model is depicted as in Fig. 2. The boundary conditions applied with equation (1) are divided into two parts as follows:

1. Heat Supply Boundary Conditions:
 - a. $T=T_o$ at $z=0$

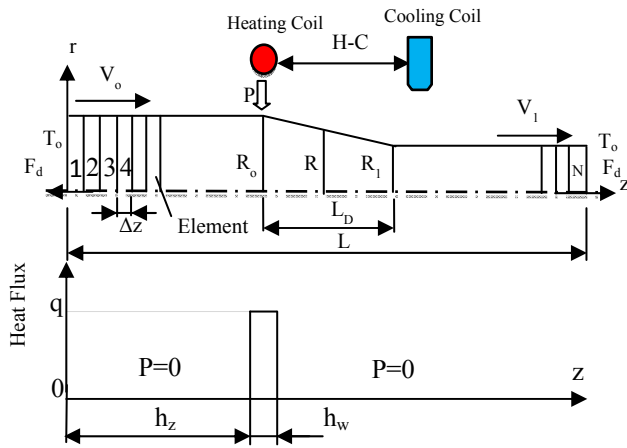


Fig. 2: Schematic of Heat Model.

- b. $T=T_o$ at $z=L$
 - c. $P=q$ at $h_z \leq z < (h_z + h_w)$
 - d. $P=0$ at $(h_z + h_w) \leq z \leq h_z$

2. Heat Transfer Coefficient Boundary Conditions:
In this model, Symmetric air cooling mode was suggested and symmetric trapizode profile is assumed for the heat transfer coefficient distribution as illustrated in Fig.3, so the boundary conditions of heat transfer coefficient are specified at three regions as follows:

- a. outside the cooling coil and the cooling air is not effective:
 $h = h_a$ at $(c_z + c_w + c_e) \leq z < (c_z - c_e)$
- b. outside the cooling coil and the cooling air still effective:
 $h = \frac{(h_c - h_a)}{c_e} \{z - (c_z - c_e)\} + h_a$ at $c_z - c_e \leq z < c_z$
 $h = \frac{(h_c - h_a)}{c_e} \{(c_z + c_w) - z\} + h_c$ at $c_z + c_w \leq z < c_z + c_w + c_e$
- c. under the cooling coil:
 $h = h_c$ at $c_z \leq z < c_z + c_w$

For more details regarding the heat transfer model, the reader can refer to the Appendix.

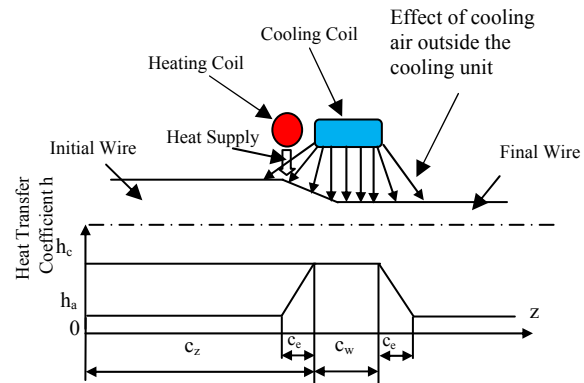


Fig. 3: Boundary Conditions of Heat Transfer Coefficient.

The thermal properties of SUS304 Stainless Steel Wire is given in Table 1.

Table 1: Thermal Properties of SUS304 Wire [21].

Property	Value
Thermal Conductivity k [W/(m.K)]	17
Specific Heat C_p [J/(kg.K)]	500
Mass Density ρ [kg/m ³]	8000
Thermal Diffusivity λ [m ² /s]	4.25E-6

2.2 DEFORMATION MODEL

During the superplastic flow, as the case in dieless drawing, the flow stress formula equation (2) is function of the temperature, strain and strain rate [22] and can be used to predict the radius profile as will be stated later. In this model, the wire radius profile is predicted and corresponding drawing force is determined based on suitable temperatures distribution supplied from the heat model. Following assumptions are considered for this model:

1. Material treated as incompressible and isotropic.
2. The stress state is (uniaxial loading) $\sigma = \sigma(z)$ and as well as velocity field.
3. Plasticity is dominated and elasticity is neglected.
4. The plane cross-section is assumed here.
5. The Drawing force is constant during deformation process.
6. The material properties: K , n and m are temperature dependent.
7. Plastic strains are dominated and thermal strains are ignored.

The following equations (2-5) are used in derivative the radius profile equation $R(z)$ [21]:

Flow stress: $\sigma = K(\epsilon_o + \epsilon)^n (\dot{\epsilon}/\dot{\epsilon}_o)^m \tag{2}$

ϵ_0 is mostly assumed as $1 s^{-1}$, ϵ_0 : is the offset strain which is assumed 0.01 to prevent zero stress state at zero strain [19].

$$\text{Strain rate: } \dot{\epsilon} = -2V_0 \frac{R_0^2}{R^3} \frac{dR}{dz} \quad (3)$$

$$\text{Drawing force: } F_d = \sigma_0 A_0 = \sigma_1 A_1 = \sigma A = \text{const.} \quad (4)$$

$$\text{Plastic strain: } \epsilon = 2 \ln \frac{R_0}{R} \quad (5)$$

Thus, the radius profile equation can be obtained as:

$$\frac{dR}{dz} = - \frac{R^3}{2V_0 R_0^2} \left\{ \frac{F_d}{K \left(\epsilon_0 + 2 \ln \frac{R_0}{R} \right)^n A} \right\}^{1/m} \quad (6)$$

Equation (6) was solved numerically by means of 5th order Runge-Kutta-Fehlberg with the following boundary conditions as can be seen from Fig. 4:

$$R=R_0 \quad \text{at } z=0$$

$$R=R_1 \quad \text{at } z=L$$

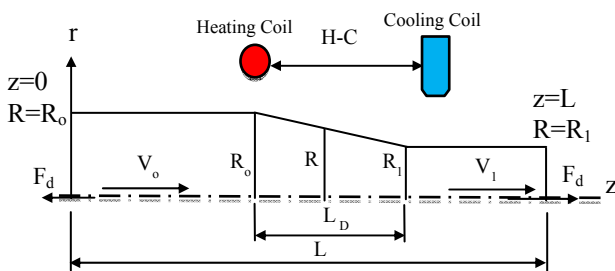


Fig. 4: Layout of Deformation Model

For more details regarding the deformation model, the reader can refer to the Appendix.

The formulas for material properties K, n and m are temperature dependent and given as [6]:

$$K(T) = 0.0007T^2 - 2.1417T + 1788.3 \quad (7)$$

$$n(T) = 4.645e-7T^2 - 3.628e-4T + 4.367e-1 \quad (8)$$

$$m(T) = 4.374e-5T + 1.449e-3 \quad (9)$$

3. EXPERIMENTAL WORK

To validate the numerical model, a comprehensive experimental program has been executed for SUS304 wire with diameter of (1.6-2) mm. For this purpose, a continuous dieless drawing machine has been designed, constructed and commissioned by the authors as depicted in Fig. 5.

3.1 DLD MACHINE DESCRIPTION

The following devices were used in construction of DLD machine; two motors-gearboxes (1 HP with 71 speed ratio) were used to generate suitable feeding and drawing speeds. Two separated variable frequency drives (1 HP) with two rotary shaft encoders (1024 ppr) were utilized to control motors-gearboxes speeds by means of PID controller through U3-HV LabJack USB data-acquisition and Microsoft Visual Studio installed on laptop computer. The PID controller constants were tuned manually with suitable values [24]. For heating the stainless steel wire, a high frequency induction heater machine (160 kHz and 16 KVA) remotely operated by the computer was used as heating source to ensure even heating of the wire. Compact cooling tower was used to cool the water entering the induction machine. K-type 1200 °C thermocouples were utilized for

measuring the temperature distribution along the wire longitudinal axis. A thermocouple temperature transmitters (4-20 mA) were connected to the thermocouples to transmit the thermocouple signals to the LabJack and then to read by the visual software. For cooling the heated wire, a 4-bar air compressor was used. The pressure of compressed air was set up to be (1.5-2 bar). The compressed air was cooled by the water cooling tower before arrive to the heated wire. In the cooling unit, the wire is passed through a sleeve pipe – having diameter of 25.4mm - which is open from both sides so as cooling air is spread. The sleeve pipe having a side aperture with diameter of 6mm is setup next to the wire in order to the cooling air coming from the compressor can impinge the wire directly and spread over it. To measure the drawing force, an S-type high sensitivity load cell with capacity of 300kg (3000N) was used. The diameter variations of drawn wire was measured on-line by a laser diameter gauge with accuracy of 0.001µm. All sensed signals such as motors signals, thermocouples signals, load cell signals and laser diameter gauge signals were transmitted through a data acquisition system U3-HV LabJack and then to the Microsoft Visual Studio to read/collect required data and control the drawing process remotely. The Visual Studio software is responsible for operating the motor-gearbox, induction heater, load cell and laser diameter gauge, whereas, cooling tower and air compressor are operated separately. The input parameters through Visual studio are feeding and drawing velocities only. The heating voltage for the induction heater is setup manually. The output data collected though Visual studio are temperatures distribution over the heated wire, drawing force and final wire diameter.

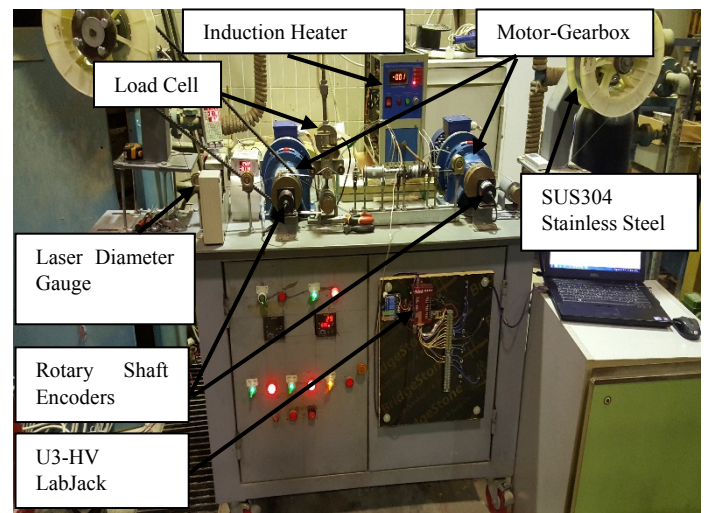


Fig. 5: Dieless wire drawing machine.

3.2 EXPERIMENT PROCEDURE

The current experimental program was devoted to study the DLD process parameters such as feeding and drawing speeds, heat flux supplied by induction coil to the wire, heating coil width and distance between heating and cooling units. Due to the low frequency of induction heating machine and paramagnetic of SUS304 stainless steel, a number of steel sleeves with different diameters and thickness were used for heating the wire passing through it

to an elevated temperature depending on supplied heat flux from induction coil. By using number of K-type thermocouples, the temperature over the sleeve surface was measured experimentally at two points only outside the heating coil, while, it was measured over the moving wire at seven points including cooling area for case-1 and at five points for case-2 and case-3 as shown in Fig. 6.

The temperature of the wire while moving it through the heating coil was difficult to measure by using a thermocouple nor infrared thermometer due to effect of magnetic field, so, a special infrared thermometer was unavailable to do that. Also, it is difficult to make a PID control on power delivered from the induction machine because its working only by on/off and there is no linear control signal allowed. Instead the power supplied from the induction machine was adjusted manually for each test. The steps of the experiment can be summarized as follows:

- 6- Start the drawing process by setting up a suitable value for the drawing speed according to the specified reduction ratio.
- 7- Monitor distribution of drawing force, temperatures and final diameter while the drawing process is continue.
- 8- Once the above parameters are steady and the wire's diameter is reduced to the target value, then it is decided that the drawing process is passed.
- 9- Stop the Visual Studio and save the acquired data for the drawing force, temperatures, and final diameter.
- 10- Power off the system.
- 11- A new tests are carried out by changing the values of drawing speed, heating coil width and heating-cooling units separation distance and then repeat the steps from 5-10.

In the experiment, the total area reduction, total strain and total strain rate were determined according to the following equations [10]:

$$RA = \frac{A_0 - A_1}{A_0} = 1 - \frac{A_1}{A_0} = 1 - \frac{V_0}{V_1} \quad (10)$$

$$\text{Total strain: } \epsilon = 2 \ln \frac{R_0}{R_1} = \ln \frac{V_1}{V_0} \quad (11)$$

$$\text{Total strain rate: } \dot{\epsilon} = \frac{\epsilon(V_0 + V_1)}{2L_D} \quad (12)$$

4. ANN MODEL

The multi-output ANN model based on the back propagation algorithm was utilized to predict the rational relationship between the input and output parameters. The MatLab software was used in constructing and executing the ANN model. The input parameters of ANN were: initial wire diameter d_0 , feeding velocity V_0 , drawing velocity V_1 , heating-cooling distance H-C, heating coil width h_w , outer diameter of heating sleeve D_s and measured heat flux q , whilst, the output parameters from ANN model were 2 parameters including; final wire diameter d_1 and drawing force F_d .

The total experimental data which used in ANN model was 34 sets. A 24 sets of them used for the training process and 10 sets utilized for the testing of the data.

Among 50 trails were performed through ANN model, the best ANN structure was (7-12-2), which has seven neurons against input layer, twelve neurons against hidden layer with tan-sigmoid activation function and two neurons against output layer with linear activation function. The coefficient of determination (R^2) was obtained for training and testing patterns for each combination, in order to, the relationship between experimental and predicted ANN output results are established. The best value of these coefficients were 0.99989 and 0.99722 for training and test data respectively against mean squared error (MSE) of 0.0147.

Also, to measure the performance and predictability of ANN model, the predicted error and mean predicted error were calculated for the best chosen structure as shown in table (2).

Table 2: Experimental and ANN Model for Prediction of Final Wire Diameter and Drawing Force

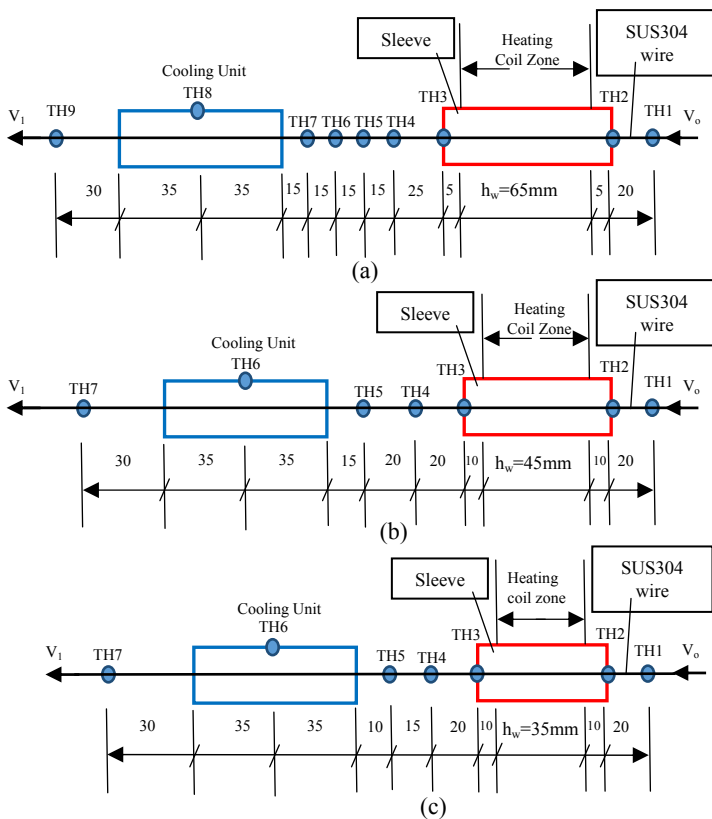


Fig. 6: Temperatures Measurement in Experiment, (a) case-1, (b) case-2 and (c) case-3. All dimensions in mm.

- 1- Power on the system.
- 2- Operate the water cooling tower to cool the induction machine before operate it for 5 minutes as recommended.
- 3- Operate the air compressor and set up the output pressure to (1.9-2) bar.
- 4- Start the Visual Studio Monitor and enter an equal values for feeding and drawing speeds firstly before start the drawing process and run the program.
- 5- Set up a suitable value for the heating voltage of the induction heater at beginning the test and waiting around (150-200) seconds until the temperature is equal to $0.4T_m$ or greater and temperatures distribution are stable along the wire.

S/N	Exp. Final Dia. [mm]	Pred. ANN Final Dia. [mm]	Error %	Exp. Drawing Force [N]	Pred. ANN Drawing Force [N]	Error %
1	1.44	1.4429	0.20139	696	711.2514	2.19129
2	1.45	1.4373	0.87586	656	650.5579	0.82959
3	1.42	1.3891	2.17606	779	765.2219	1.76869
4	1.3	1.3090	0.69231	255	257.9337	1.15047
5	1.41	1.4730	4.46809	376	297.5152	20.8736
6	1.28	1.2839	0.30469	390	391.4771	0.37874
7	1.72	1.7070	0.75581	482	440.7288	8.56249
8	1.63	1.6243	0.34969	462	472.4965	2.27197
9	1.6	1.6018	0.1125	508	512.3910	0.86437
10	1.6	1.5431	3.55625	612	638.0090	4.24984
Mean Error % = 1.349			Mean Error % = 4.314			
$\text{Error (\%)} = \frac{ \text{actual value} - \text{predicted value} }{\text{actual value}} \times 100$						
$\text{Mean Error (\%)} = \frac{1}{p} \sum_{i=1}^p \left(\frac{ \text{actual value} - \text{predicted value} }{\text{actual value}} \times 100 \right)$						

5. RESULTS AND DISCUSSION

5.1 EXPERIMENTAL AND NUMERICAL RESULTS

In the experimental procedure, more than 95 tests were performed and only 34 tests were passed successfully. Three cases were taken for h_w and H-C, namely, $h_w=65\text{mm}$, H-C=90mm for case-1, $h_w=45\text{mm}$, H-C=65mm for case-2 and $h_w=35\text{mm}$, H-C=55mm for case-3. Also, symmetric cooling mode was applied which mean that cooling unit is opened from both sides to spread cooling air far distance along the wire and heating sleeve. Samples of passed wires are presented in Fig. 7. The range of feeding speed which used in the experiments was (2.1-3.139) mm/s, whereas, the drawing speed was in the range (3.27-4.971) mm/s. The maximum reduction in diameter was 1.26mm against area reduction ratio of 37.9% for the original diameter of 1.6mm. For the other diameter 2.0mm, the maximum reduction was 1.54mm against 40.7% reduction ratio.



Fig. 7: Photos of passed wires produced by present DLD machine.

Effect of feeding velocity on the drawing force is shown in Fig.8. Distinctly, the drawing force was raised up with increased feeding velocities. By increasing the feeding velocity, the strain rate also is increased resulting in

increase of the flow stress. Consequently, the drawing force is increased. Fig. 9 shows effect of heating coil width h_w and H-C separation distance on the drawing force. Since, the high temperature zone give rise to reducing the wire strength and raising its ductility, where, least flow stress and supreme strain rate take place at maximum temperature point. The same was reported by [18]. Further, when decreasing the heating coil width and H-C distance, the drawing force was raised up due to regression of high temperature region and spreading of high cooling rate towards heated wire. Effect of feeding velocity on wire profile for both numerical and experimental results is shown on Fig. 10. Clearly, the strain rate was increased due to increased drawing velocity;

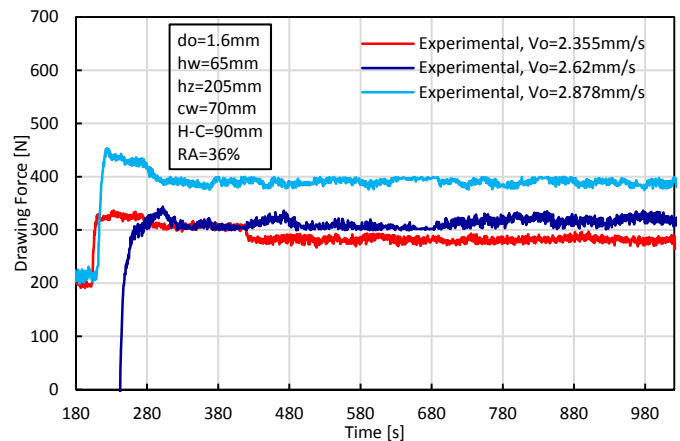


Fig. 8: Effect of Feeding Velocity V_o on Drawing Force.

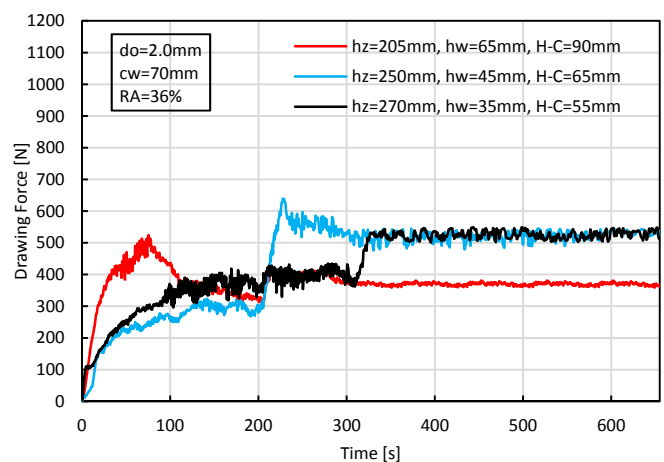


Fig. 9: Effect of Heating Coil Width h_w and H-C Distance on Drawing Force.

this led to extension of deformation zone somewhat for increased feeding velocities. The same behavior was noticed with some differences in profile at the deformation area. As seen from this figure that profile of wire diameter was descended in gradual to the desired diameter for the numerical simulation, whilst, the descending was steep for the experimental one. It is suggested that the experimental temperatures drop was steepest due to heat losses from the sleeve and effect of cooling air coming from cooling unit towards heating coil. This can explain why experimental wire profile was steepest.

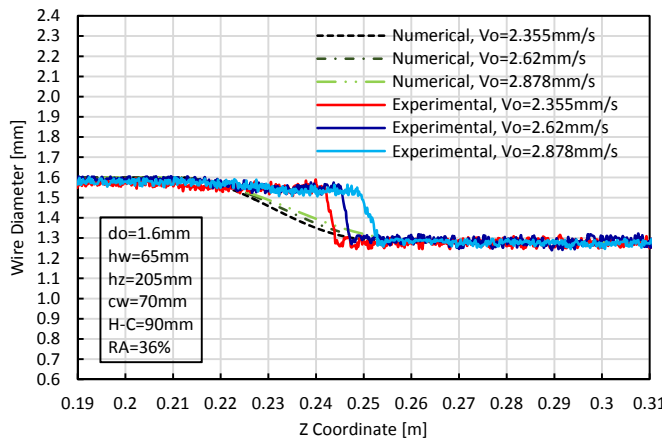


Fig. 10: Numerical and Experimental Wire Profile at Different Feeding Velocities.

Influence of heating coil width and H-C distance on wire profile is explained numerically and experimentally as in Fig. 11. Also, the same behavior for the numerical and experimental profiles was found excluding some variances in the deformed zone as stated above in Fig. 10.

This evidently proves that with increasing of heating coil width and H-C distance, the deformation zone is extended more. Widen the heating coil will contribute in delivering more heat to the wire by expanding the high temperature region. In fact, while the deformed area is longer, the time required for deformation become also longer leading to decreasing the strain rate there. By this way, more reduction in area can be suggested by expanding the deformation zone. On the other hand, effect of cooling air becomes less with increasing H-C distance which allows in turn more deformation to occur. This was agreed with what suggested by [13, 14].

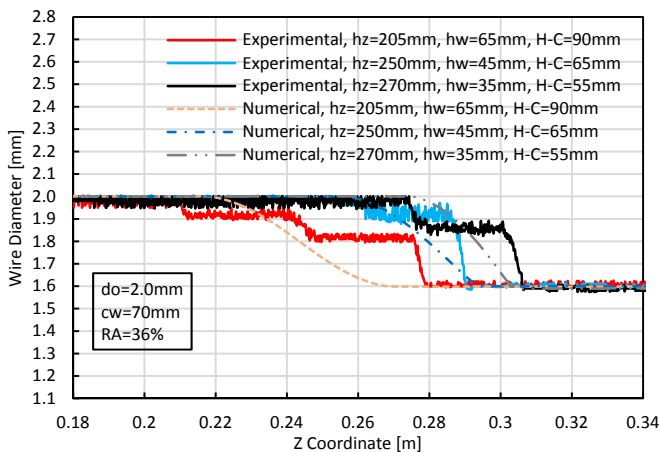


Fig. 11: Numerical and Experimental Wire Profile at Different Heating Coil Width and H-C Distance.

Fig. 12 explains the relationship between wire profile and reduction ratio. Obviously, the wire profile was affected by increasing the reduction ratio, and reduced to the specified diameter. Also, noted that at constant heat flux and feeding velocity, all profiles had similar behavior along with deformation area. It is confirmed that strain rate was decreased during long deformation zone which in turn improved reduction ratio. This is agreed with other authors who worked on DLD process. Also, good agreement was remarked between numerical and experimental profiles.

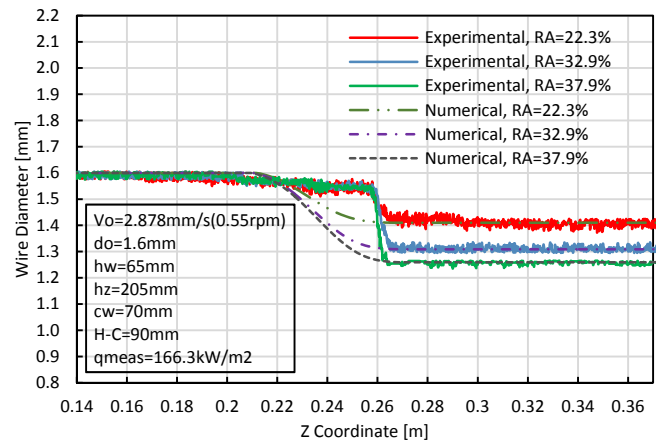


Fig. 12: Relationship between Wire Profile and Reduction Ratio.

Fig. 13 shows the relationship between strain rate and heating coil width. It is apparent that strain rate was effected by reducing the width of heating coil, since the time required to carry out the forming process along the deformation zone was reduced. This is acceptable from the physical standpoint, since, to achieve the same amount of deformation, once through small distance and another through larger distance, surely, the deformation time is shorter and deformation rate is larger for the first case than a second case.

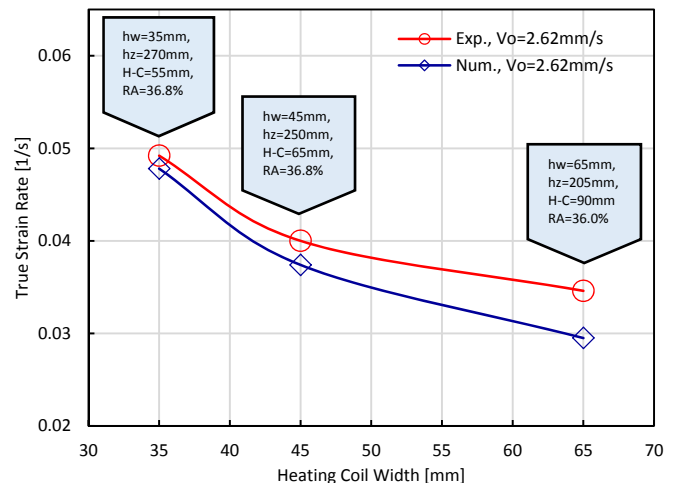


Fig. 13: Relationship between True Strain Rate and Heating Coil Width.

Fig. 14 states effect of increasing of feeding velocity on flow stress. It is pronounced that flow stress was increased with increasing of feeding velocity. Increasing of flow stress may attributed to raising of level of strain rate due to feeding velocity. Even though, levels of flow stress are reduced at elevated temperatures, but increasing of rate at which deformation occurs (strain rate) implied an intensely motion of the material microstructure which necessitated an increase in the flow stress.

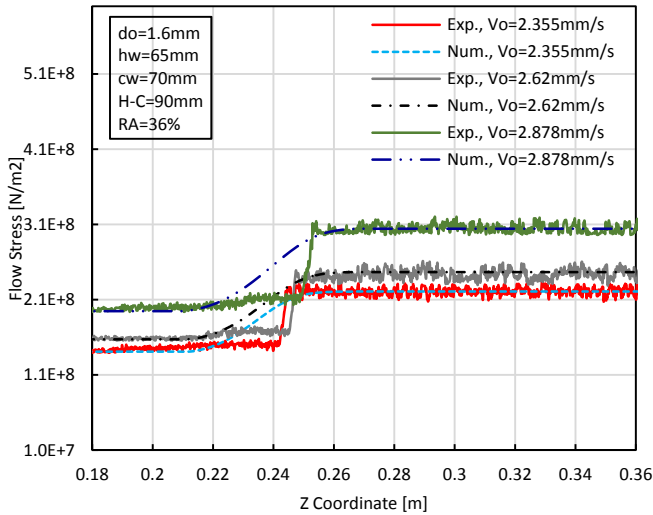


Fig. 14: Effect of Feeding Velocity on Flow Stress.

5.2 COMPARISON OF EXPERIMENTAL, NUMERICAL AND ANN RESULTS

The following discussion displays the performance of ANN model and comparison with experimental and numerical results. Figs. (15-16) show the best fit line –coefficient of determination R^2 – for prediction of final diameter and drawing force of training and testing data respectively. With high value of R^2 close to unity for both training and testing data, the best performance of ANN can be expected.

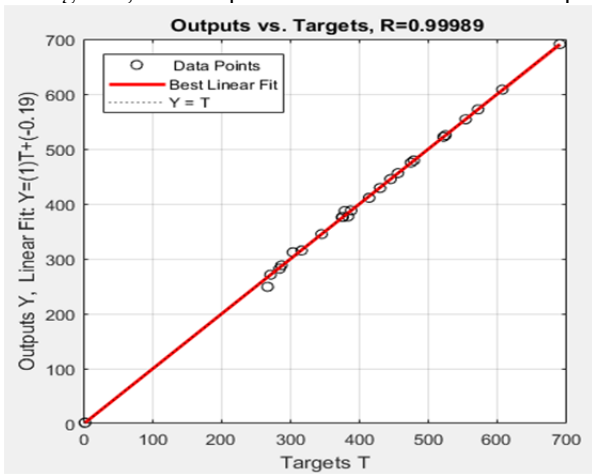


Fig. 15: Best Fit Line for Prediction of Final Diameter and Drawing Force by ANN Model for Training Samples.

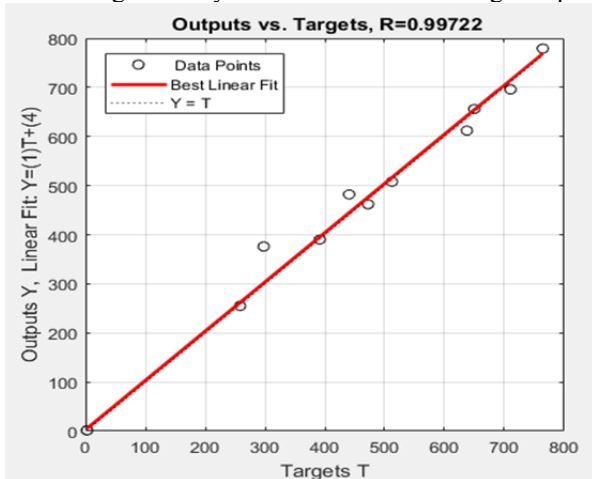


Fig. 16: Best Fit Line for Prediction of Final Diameter and Drawing Force by ANN Model for Testing Samples.

Figs. (17-18) display the comparison between experimental and predicted output results for the final diameter and drawing force respectively. As seen from these two figures, that ANN model was able to predict outputs close to experimental values for the final wire diameter and drawing force with good agreement.

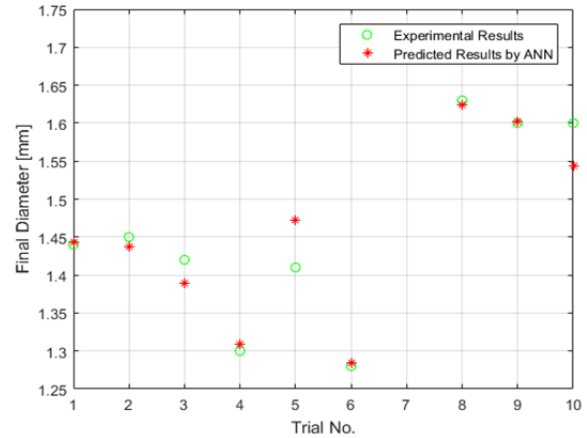


Fig. 17: Comparison of Experimental and Predicted ANN Results of Final Wire Diameter.

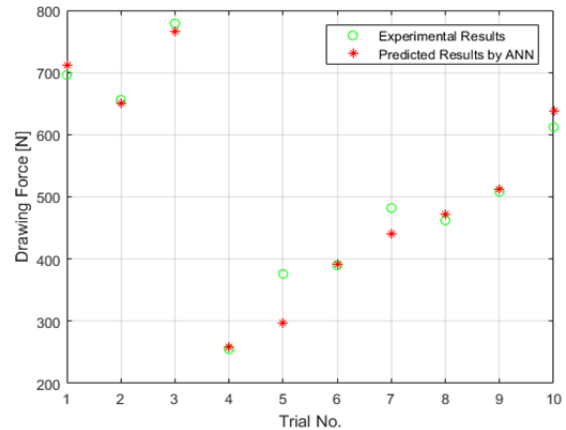


Fig. 18: Comparison of Experimental and Predicted ANN Results of Drawing Force.

Fig. 19 shows the relationship between final diameter and drawing velocity. Visibly, increasing of the drawing velocity led to decreasing the wire diameter. This is because increasing the stain and strain rate with increasing the forming velocity.

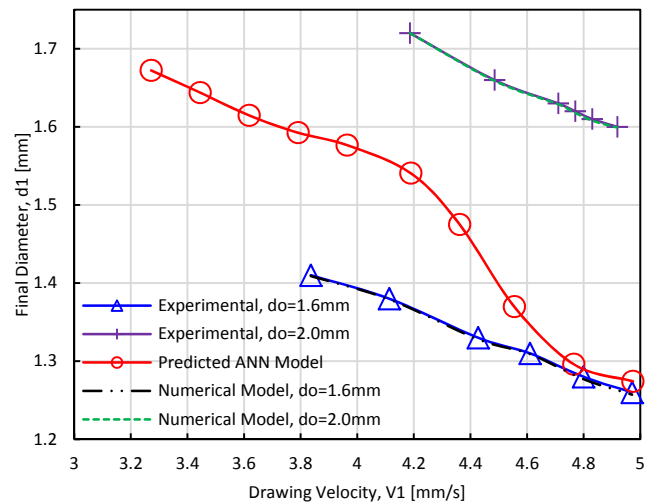


Fig. 19: Effect of Drawing Velocity on Wire Diameter.

Effect of drawing velocity on drawing force at constant heat flux is illustrated by Fig. 20. At constant heat flux, increasing the drawing velocity will increase the strength of wire due to increase of strain hardening, consequently, the drawing force is increased. Also, increasing of drawing velocity will increase the strain rate which in turn leads to increase of flow stress and drawing force accordingly.

Fig. 21 shows effect of heat flux on drawing force. By increasing the heat flux, the wire becomes more ductile and its strength decreases more, since flow stress is decreased and this requires less drawing force to make deformation and reducing the wire diameter.

It is shown from Figs. (19-21) that ANN model could predicts the same behavior as experimental and numerical results with good agreement as indicated. The foregoing discussions can be useful here to explain this attitude for these figures.

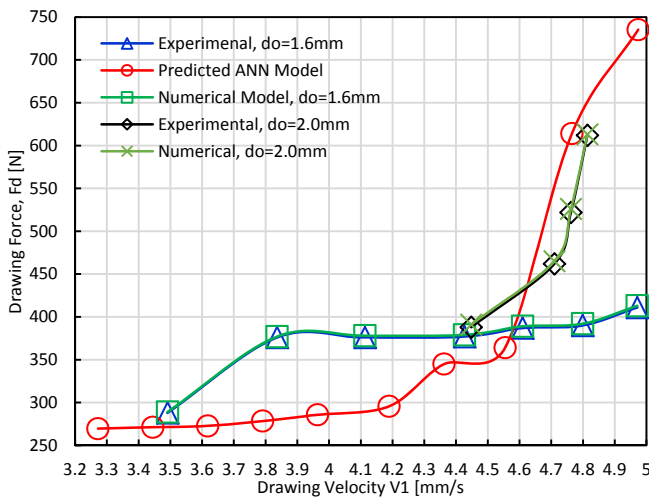


Fig. 20: Effect of Drawing Velocity on Drawing Force.

Fig. 22 explains the relationship between feeding velocity and drawing force for experimental, numerical and ANN results. The same behavior is noted for ANN, numerical and experimental results. Effect increasing of feeding velocity on drawing force was discussed above as in Fig.8.

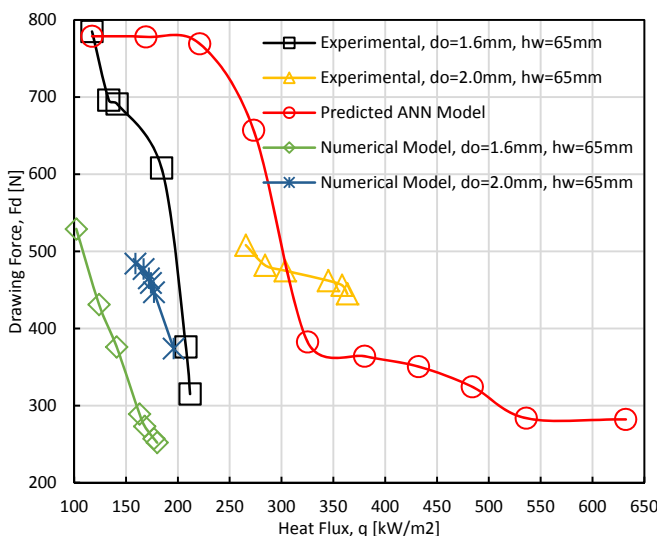


Fig. 21: Effect of Heat Flux on Drawing Force.

Fig. 23 states the relationship between heating coil width h_w and drawing force for experimental, numerical and ANN results. Also, it is noted that there

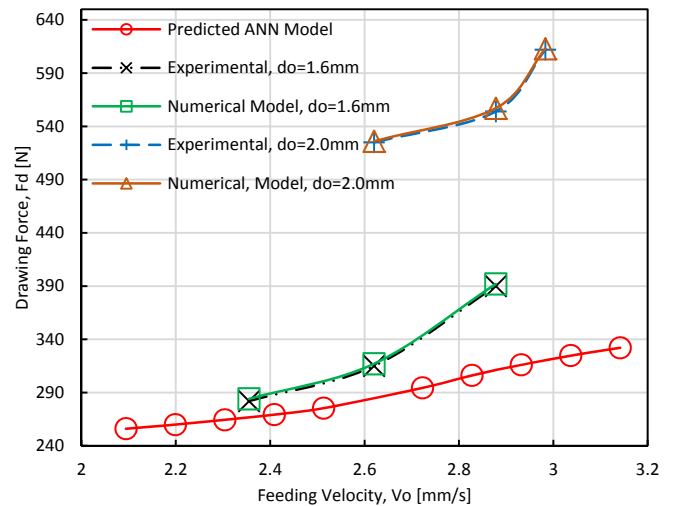


Fig. 22: Effect of Feeding Velocity on Drawing Force.

is good agreement among the results. Effect of heating coil width also was discussed above as in Fig. 9.

It is noted when comparing results of ANN model with numerical and experimental results, that there is some deviation but the behavior is the same. This deviation can be attributed to the range of data which ANN model is based on, since the ANN model included the whole range of the experimental data. On other hand, the results of experimental and numerical model which compared with ANN results included specific range of the data not the whole range.

It is suggested here that ANN model having an effective tool to predict the DLD process behavior within the range of the current experimental data.

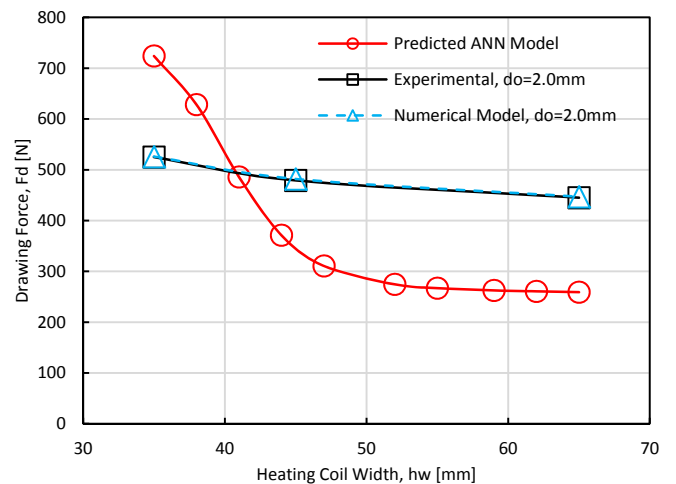


Fig. 23: Effect of Heating Coil Width h_w on Drawing Force.

6. CONCLUSION

This paper is dedicated to study the continuous dieless wire drawing process for SUS304-Stainless Steel wire having diameter of (1.6-2) mm. A special continuous dieless drawing machine has been successfully designed, constructed and commissioned to study DLD process parameters. Besides, a numerical model has been developed and validated with the experimental results. Also, ANN model was prepared to predict the DLD process parameters. The following notes can be deduced:

1. A maximum area reduction of 40.7% and 37.9% for 2mm and 1.6mm initial diameter respectively was achieved.
2. A final diameters of 1.26mm and 1.54mm of original diameters of 1.6mm and 2mm respectively were obtained experimentally.
3. A maximum feeding speed of 3.139mm/s was recorded whereas, a maximum drawing speed of 4.971mm/s was realized.
4. It is confirmed that drawing force was increased by increasing the feeding velocity and decreased by increasing the supplied heat flux. Consequently, the flow stress is also effected accordingly.
5. The drawing force also was decreased by widen the heating coil and increase the H-C distance.
6. It is remarked that drawing force was increased by increasing the drawing velocity at constant heat flux.
7. The deformation zone length was extended by increasing the feeding velocity due to increased strain rate accordingly.
8. It is noted that wire profile was steep rather than gradual by decreasing the heating coil width and H-C distance due to high cooling rate and regression of deformation zone.
9. It is confirmed that levels of strain rate was reduced by increasing the heating coil width and H-C distance.
10. It is confirmed that reduction ratio was promoted at constant feeding velocity and heat flux due to low levels of strain rate at heating coil width of 65mm.
11. It is suggested that ANN model can predict the behavior of DLD process within present experimental data.

7. APPENDIX

Heat Transfer Model: Fig. 24 shows the flow chart of this model. All variables read by this model are based on the current experimental data including the T_{sp} which is corresponding to the maximum temperature which measured experimentally. Also, based on the experimental data, h_a and h_c are calculated based on the free convection and crossflow convection relations [23]. The total amount of the heat flux is determined at stop of the program.

Deformation Model: Fig. 25 shows the flow diagram of this model. Also, all parameters read by this model are based on the experimental data. An intial value for the drawing force is assumed and then the final value is calculated at stop of the program.

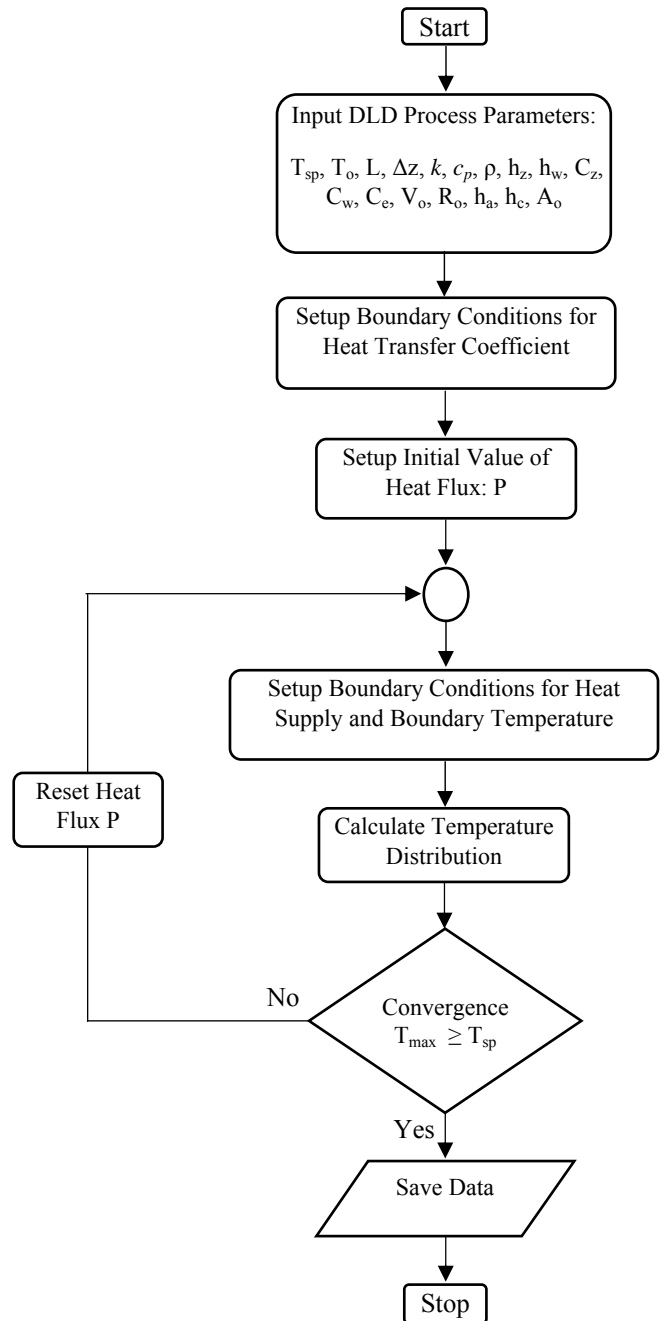


Fig. 24: Flow Chart of Heat Transfer Model.

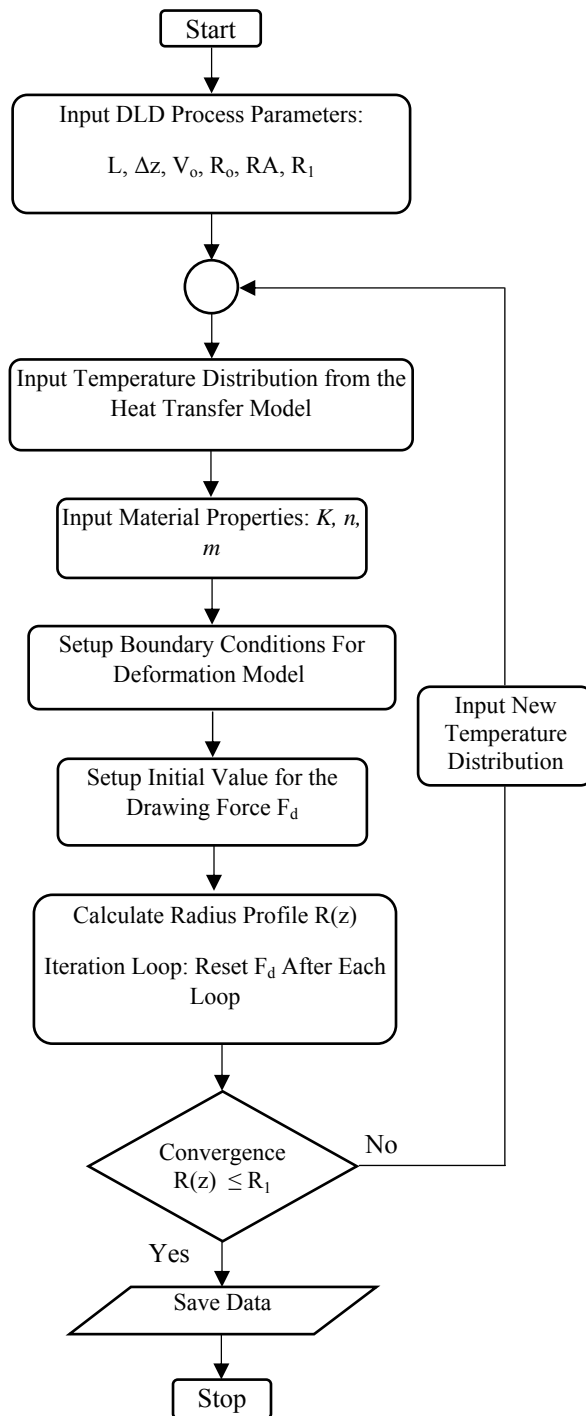


Fig. 25: Flow Chart of Deformation Model.

8. REFERENCES

- [1] J. M. Alexander and T. W. Turner, "A preliminary investigation of the die-less drawing of titanium and some steels," Proc. Mach. Tool Des. Res., vol. 15, pp. 525-537, 1974.
- [2] K. Sekiguchi, H. Kobatake, and K. Osakada, "A fundamental study on dieless drawing," Proc. Mach. Tool Des. Res., vol. 15, pp. 539-544, 1974.
- [3] M. S. J. Hashmi, G. R. Symmons, and H. Parvinmehr, "A novel technique of wire drawing," Arch. J. Mech. Eng. Sci. 1959-1982 (vols 1-23), vol. 24, no. 1, pp. 1-4, 1982.
- [4] U. Weidig, R. Kaspar, O. Pawelski, W. Rasp, "Multiphase microstructure in steel bars produced by dieless drawing," steel research, Vol. 70, No. 4-5, pp. 172-177, 1999.
- [5] O. Pawelski, W. Rasp, K. Schmeisser, "Dieless Drawing — A Forming Process Allowing Flexible Shape Generation," In: Kochhar A.K. (eds) Proceedings of the Thirty-First International Matador Conference, Palgrave, London, DOI: https://doi.org/10.1007/978-1-349-13796-1_61, pp. 401-406, 1995.
- [6] K. J. Fann, C. F. Yu, C. H. Chang, "Analysis of dieless drawing to form the end of metal wires under proportional shape evolution with Slab method," Trans Tech Publications, Switzerland, Materials Science Forum, vol. 920, pp. 155-160. 2018.
- [7] Y. Hwang, T. Kuo, "Dieless Drawing of Stainless Steel Tubes," International Journal of Advanced Manufacturing Technology, vol. 68, pp. 1311-1316, 2013.
- [8] Y. M. Hwang, Z. S. Li, T. Y. Lin, "Formability Discussion in Dieless Drawing of Stainless Steel Tubes," Trans Tech Publications, Switzerland, Key Engineering Materials, vol. 626, pp. 10-15, 2015.
- [9] Z. T. Wang, S. H. Zhang, Y. Xu, G.F. Luan, G. R. Bai, "Experiment Study on the Variation of Wall Thickness During Dieless Drawing of Stainless Steel Tube," Journal of Materials Processing Technology, vol. 120, issues 1-3, pp. 90-93, 2002.
- [10] P. Tiernan, M. T. Hillery, "An analysis of wire manufacture using the dieless drawing method," Journal of Manufacturing Processes, Vol. 10, pp. 12-20, 2008.
- [11] Y. Huh, B.K. Ha, J.S. Kim, "Dieless drawing steel wires using a dielectric heating method and modeling the process dynamics," Journal of Materials Processing Technology, vol. 210, pp. 1702-1708, 2010.
- [12] M.D. Naughton, P.Tiernan, "An experimental analysis of the dieless drawing process (Variant B) using ELI grade Ti-6AL-4V wire alloy," Proc. IMechE Vol. 222 Part B: J. Engineering Manufacture, pp. 225-236, 2008.
- [13] M.D. Naughton, P.Tiernan, "An experimental approach to continuous dieless wire drawing (Variant A) using ELI Ti-6AL-4V alloy," Journal of Engineering Materials and Technology, Vol. 131, pp. 1-10, 2009.
- [14] T. Furushima, Y. Noda, K. Manabe, "Effective Heating Conditions for High Speed Dieless Tube Drawing Process", Steel Research International, Vol. 81, No.9, pp. 502-505, 2010.
- [15] T. Furushima, Y. Imagawa, S. Furusawa, K. Manabe, " Deformation profile in rotary laser dieless drawing process for metal microtubes ", Procedia Engineering, Vol. 81, pp. 700-705, 2014.
- [16] W. Hongyu, J. Shijun, Z. Dwen, Z. Dianhua, "Analysis and study of dieless drawing process for rod based on radial direction gradient slab method," The International Journal of Advanced Manufacturing Technology, Springer-Verlag London Ltd., Vol. 98, Issue 1-4, pp. 839-847, 2018.
- [17] T. Furushima, K. Manabe, "Large Reduction Die-less Mandrel Drawing of Magnesium Alloy Micro-Tubes ", Science Direct, CIRP Annals - Manufacturing Technology, Vol. 67, Issue 1, pp. 309-312, 2018.

- [18] F. M. R. Fortunier, H. Sassoulas, "A Thermo-Mechanical Analysis of Stability in Dieless Wire Drawing," *Int. J. Mech. Sci.*, vol. 39, no. 5, pp. 615–627, 1997.
- [19] H. Jafari, "Thermo-Mechanical Investigation of Die-Less Wire Drawing Process," MSc Thesis, University of British Columbia, Vancouver, 2013.
- [20] T. Furushima, T. Ikeda, Y. Noda, K. Manabe, "Deformation and Heat Transfer Analysis of Dieless Drawing Process for Metal Tube," Wiley-VCH Verlag GmbH & Co. KGaA. Weinheim, *Steel Research Int. Special Edition*, pp. 302-307, 2011.
- [21] Rafid Jabbar Mohammed, Jaafar Khalaf Ali, Ameen Ahmed Nassar, "Numerical Analysis of Continuous Dieless Wire Drawing Process," *International Journal of Engineering and Technology*, Vol. 7, No. 4.19, pp. 699-704, 2018.
- [22] K.A. Padmanabhan, R.A. Vasin, F.U. Enikeev, "Superplastic Flow: Phenomenology and Mechanics," Springer-Verlag Berlin Heidelberg, 2001.
- [23] J.P. Holman, "Heat Transfer", McGraw-Hill Companies, Inc., 9th edition, 2002.
- [24] W. S. Levine, "The Control Handbook", Vol. 1, CRC Press Inc., 2000.